Editors' Suggestion

Quectonewton Local Force Sensor

Yann Balland, Luc Absil, and Franck Pereira Dos Santos
LNE-SYRTE, Observatoire de Paris, Université PSL, CNRS, Sorbonne Université, 61 avenue de l'Observatoire, 75014 Paris, France

(Received 21 October 2023; accepted 12 August 2024; published 13 September 2024)

We report on the realization of a quantum sensor based on trapped atom interferometry in an optical lattice for the measurement of atom-surface interactions, with sub-micrometer-level control of the mean atom-surface separation distance. The force sensor reaches a short-term sensitivity of 3.4×10^{-28} N at 1 s and a long-term stability of 4 qN (4×10^{-30} N). We perform force measurements in the 0–300 μm range, and despite significant stray forces caused by adsorbed atoms on the surface, we obtain evidence of the Casimir-Polder force.

DOI: 10.1103/PhysRevLett.133.113403

Short-range forces are at the frontiers of modern physics [1,2]. In the submillimeter scales, quantum electrodynamics (QED) interactions dominate, and give rise in atom-surface interactions to the Casimir-Polder force [3]. Since its first highlight [4], different methods [5] have been able to bring it out, notably by measuring the transmission of an atomic beam through a micron-sized cavity [6], diffracting matter waves on a surface [7] or performing spectroscopy in vapor cells [8,9]. However these approaches have struggled to achieve the sensitivity required to detect these tiny forces while maintaining a good understanding of the setup geometry, particularly, the distance separating atoms from the surface.

Few experiments achieved measuring Casimir-Polder forces while controlling directly the atom-surface distance. In the range from tens to hundreds of nanometers, the Casimir-Polder potential was measured by reflecting the atoms on an evanescent field [10,11]. In the micrometer range (around 6 μm), the Casimir-Polder effect was highlighted by tracking the oscillations of a Bose-Einstein condensate (BEC) inside a harmonic trap [12], a method that does not measure the force though, but rather its gradient. An appealing method we use here to perform spatially resolved and sensitive force measurements is to trap atoms during extended measurement times in a shallow vertical optical lattice.

The lattice potential, tilted by gravity g and any other external uniform force F_e, leads to a Wannier-Stark (WS) Hamiltonian. Its eigenstates $|W_m\rangle$ are localized in every well m of the lattice and separated by the Bloch frequency $\nu_b = (m_{\mathrm{Rb}} g + F_e)\lambda_l/(2h)$, with m_{Rb} the mass of the atom and λ_l the wavelength of the lattice beam [13] (Fig. 1). The Wannier-Stark ladder holds even if the force $F_e(z)$ is not uniform but remains perturbative relatively to the gravity force $m_{\mathrm{Rb}} g$. Different protocols have been proposed to measure Casimir-Polder forces using such optical lattices, based for instance on performing interferometry with a BEC [14] or measuring the frequency shift $\delta\nu_b$ of Bloch oscillations [15,16].

In our experiment, Raman transitions coherently couple two Wannier-Stark states Δm wells apart [17], as illustrated in Fig. 1. Two Raman $\pi/2$ pulses, separated by the evolution time T, drive a Raman-Ramsey interferometer, allowing us to measure the frequency $\Delta m\, \nu_b$, and thus the external force applied to the atoms, with the excellent sensitivity of an atomic clock. With this method, force sensitivities of 2.7×10^{-30} N or 7×10^{-30} N at 1 s were reported in [18], for atomic sample sizes of, respectively, 2 mm and 3 μm. These are comparable to the sensitivity obtained with an alternative method based on the coupling induced by amplitude modulation of the lattice [19].

These two methods, demonstrated far from any surface, essentially allowed measuring gravity, with sensitivities in the $10^{-6} g$ at 1 s, way above the record sensitivities of free fall interferometers, in the $10^{-9} g$ at 1 s [20]. It is also worse,

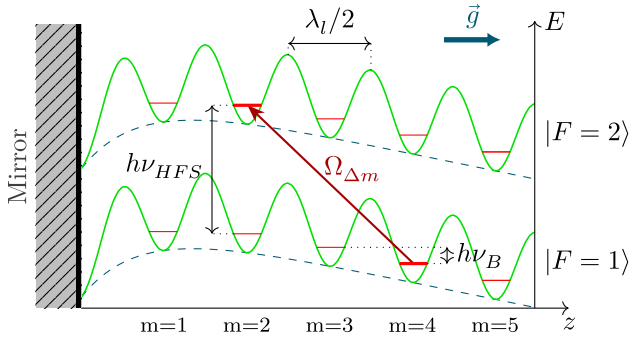

FIG. 1. Wannier-Stark ladder potential and eigenstates. Two neighboring states $|W_m, F=1\rangle$ and $|W_{m+\Delta m}, F=2\rangle$ separated by the energy $h(\nu_{\mathrm{HFS}} + \Delta m\, \nu_B)$ are coupled by Raman transitions with a Rabi frequency $\Omega_{\Delta m}$. Close to the surface, Casimir-Polder interactions modify the external potential (dashed lines) and the value of ν_B.

by about an order of magnitude, than levitated interferometers [21], where after being split in free fall by Raman pulses, separated wave packets are trapped for seconds in an optical lattice. But what sets these fully trapped force sensors apart is their spatial resolution [16,18], compared to free fall and levitated sensors [20,21] limited to the millimeter range by the initial size of the laser cooled cloud and its expansion in free fall. In our case, the resolution is limited by the size of the cloud (of 3.5 micrometers rms) and, to a lesser extent, by the extension of Wannier-Stark wave functions (three wells rms, less than a micrometer). However, no such interferometer succeeded to perform atom-surface force measurements, due either to a lack of sensitivity [16] or a loss of signal for distances as large as 1 mm from the surface [22]. By contrast, our sensor is capable of performing force measurements at much shorter distances, with a sensitivity orders of magnitudes better than previous surface force measurements using trapped ions [23], nanospheres [24] or macroscopic devices [25].

We present here the main features of our local force sensor and evaluate its performance. We demonstrate a short-term sensitivity of 3.4×10^{-28} N at 1 s and a long-term stability of 4×10^{-30} N on the force measurements, allowing to measure interaction forces at the percent level in the range of tens of micrometers. Finally, we compare our measurements at the shortest distances, below 10 μm, with the expected Casimir-Polder force.

In our experiment, ^{87}Rb atoms are laser cooled in a magneto-optical trap, before being transferred in a crossed dipole trap. A 2 s long evaporative cooling stage leaves us with 120 000 atoms at a temperature of 300 nK, with a vertical size of 10 μm rms. Adiabatically ramping up the dipolar trap at the end of the evaporation reduces this size by a factor of 3, at the cost of heating the atoms up to 1500 nK. This preparation step is done in a first chamber, 30 cm below our surface of interest, a superpolished fused silica dielectric mirror, with customized coating highly reflective at 532 nm, but transparent at 780 and 1064 nm.

The transport of the atoms to the vicinity of this mirror is performed with a moving lattice described thoroughly in [26]. Two counterpropagating beams, red detuned from the ^{87}Rb D2 line by 250 GHz with a controlled frequency difference, create a moving lattice in which the atoms are trapped (Fig. 2). This setup allows a fine control of the transport distance Δz with a resolution in the tens of nanometers [26]. However, the distance z_{at} between the atoms and the surface is not directly known. It depends on the exact distance $z_{\mathrm{tot}} = z_{\mathrm{at}} + \Delta z$ between the dipole trap and the mirror, which varies with beam misalignments and thermal fluctuations. To calibrate this distance z_{tot}, we use the mirror surface directly as a position reference by transporting our atomic cloud in its vicinity, similarly to [16]. Since atoms kicked into the surface are lost, the exact position of the surface can be determined by measuring the number of remaining atoms, as shown in Fig. 3. Assuming a Gaussian density distribution and fitting the atom number by an erf function, we extract both the distance z_{tot} and the $1/e^2$ size of the cloud. This allows determining the atom-surface distance z with submicrometer uncertainty, limited by the fit uncertainty. Since the distance z_{tot} remains stable at the 0.1 μm level over hours but fluctuates by a few micrometers over days, we perform this distance calibration step twice an hour along the force measurements to track any fluctuation. As for the vertical

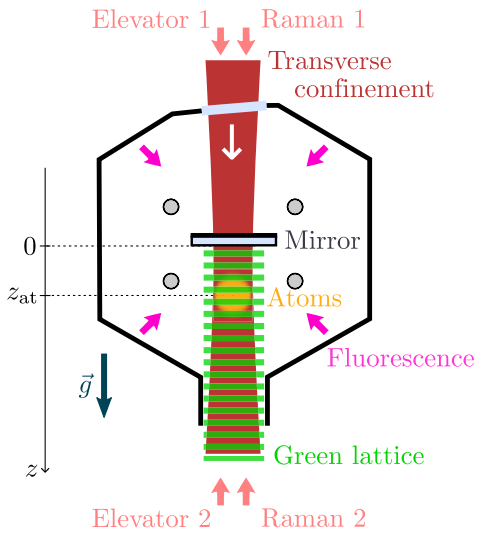

FIG. 2. Scheme of the upper chamber, with the mirror of interest at its center. Two counterpropagating beams at 780 nm ensure the transport of the atoms, while two other counterpropagating Raman beams drive the interferometer. The Raman 1 beam is actually retroreflected on a Raman mirror, not depicted here, located above the mirror of interest [27,28]. Atoms end up trapped vertically in the lattice created by retroreflecting a green laser beam at $\lambda_l = 532$ nm on the surface of the mirror, and transversally with a propagating IR beam at 1064 nm. Four linear electrodes (displayed as gray circles) are used to produce external electrostatic fields.

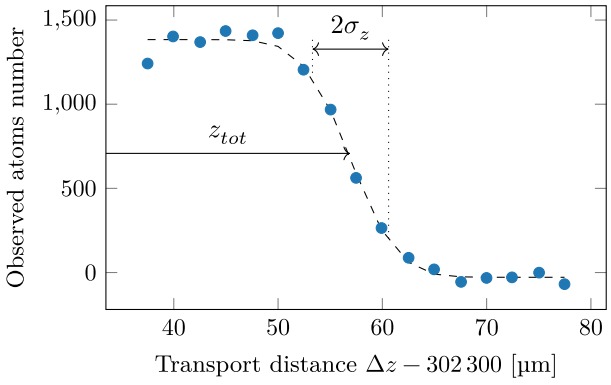

FIG. 3. Number of remaining atoms as a function of the transport distance Δz. We extract the position of the surface z_{tot} and the width σ_z of the atomic cloud from a fit to the data (dashed line).

size σ_z of the cloud, it remains unchanged during transport with a $1/e^2$ size σ_z of 3.5 μm.

We end up with 20 000 atoms at most after the transport, in a mixture of $|F=1\rangle$ and $|F=2\rangle$. Atoms in $|F=2\rangle$ are depumped in $|F=1\rangle$ before their transfer in the green static shallow lattice used for the force measurement. Being blue detuned, the light potential confines only in the vertical direction. An additional IR laser beam, propagating and red detuned, transversally confines the atoms at the center of the lattice (Fig. 2). After 500 ms trapping time, we are left with at most 1000 trapped atoms in $|F=1, m_F=0\rangle$ to perform the measurements.

Two counterpropagating Raman lasers, detuned from the D2 line by 300 GHz and coupling the $|W_m, F=1\rangle$ and $|W_{m+\Delta m}, F=2\rangle$ states for every initial well number m, are then used to drive the Ramsey interferometer that allows for measuring their energy difference [27]. They both enter the chamber at its bottom. At its top, one of the two Raman beams (Raman 2) is reflected out by a cube while the other (Raman 1) is transmitted and retroreflected on a Raman mirror [28]. This implementation ensures the stability of the Raman phase difference, whose equiphases are tied to the position of the Raman mirror. To maximize the Rabi frequency of the Raman transition $\Delta m = 6$, the static lattice is set to a depth of 1.9 recoil energy [17,28].

After the Ramsey interferometer, the two output ports being labeled by their hyperfine levels, their populations are finally measured with *in situ* state selective fluorescence imaging, using crossing pairs of retroreflected laser beams. An imaging system with a numerical aperture of 0.32 collects over 1 ms about 40 photons per atoms onto an electron multiplying CCD camera.

The interferometer phase Φ, which is derived from the output ports populations, is given by $\Phi = 2\pi(\nu_R - \nu_{\mathrm{HFS}} - \Delta m\,\nu_B)T$ where ν_R is the frequency difference between the two Raman beams and ν_{HFS} is the hyperfine splitting frequency. By tuning the Raman frequency difference to keep the output phase null, we get $\nu_R = \nu_{\mathrm{HFS}} + \Delta m\,\nu_B$. To remove the dependence on the hyperfine frequency, which can slowly fluctuate with laser light shifts, we alternately perform measurements for $\pm\Delta m$. Their difference gives the Bloch frequency free from the hyperfine frequency $\nu_B = (\nu_R^{+\Delta m} - \nu_R^{-\Delta m})/2\Delta m$.

Note that all six vertical beams (Fig. 2) overlap, in order to avoid parasitic couplings to transverse states [29]. The uncertainty in the overall vertical alignment has been reduced down to 1.5 mrad using a liquid mirror as a reference, while all beams are superimposed on one another to better than 0.1 mrad.

We now quickly discuss the limitations of the sensitivity of the force measurement. The contrast of the interferometer is typically of 40% for a coherence time of about 150 ms. We attribute the limit on coherence to unevenness of the trapping potential due to the surface, an effect which turned deleterious in a previous attempt [22]. The roughness of our mirror surface (≈1 Å rms) scatters a fraction of the trapping light and the resulting speckle adds inhomogeneities we estimated to a few 10^{-28} N close to the surface. Additionally, at less than 20 μm of the mirror, inhomogeneities of the atom-surface force further reduce the interferometer contrast.

As for the measurement noise, we identified three main contributions. The first is Raman phase noise due to vibrations of the mirror of interest relatively to the Raman retroreflecting mirror. The mirror of interest is clamped to the overall structure through an in-vaccum manipulator. Still, residual vibrations induce fluctuations on ν_B estimated at the level of 480 mHz rms per shot. We set up an optical Michelson interferometer that combines the incoming and retroreflected lattice laser beams to track the motion of the mirror of interest relatively to the optical bench. By correcting *a posteriori* the Bloch frequency measurement from the effect of this relative motion, similar to [30], the contribution of vibration noise reduces by about 30%, down to the level of 300 mHz per shot.

The second noise source is the quantum projection noise, corresponding to 200 mHz for the typical number of 500 atoms. The third is a background detection noise, equivalent to 20 atoms, which adds 190 mHz. These three contributions sum up (quadratically) to 410 mHz, which is in agreement with the measured noise of 430 mHz. Finally, since we use $\Delta m = 6$, we reach a sensitivity on the measurement of the Bloch frequency of 71 mHz/shot. Given our cycle time of 3.6 s, this corresponds to a sensitivity of 3.4×10^{-28} N at 1 s. For an averaging time of 5.5 h, the noise averages down as white noise and a long-term stability of 4 quectonewtons is reached. It outperforms any other local force measurements, even when performed far from any surface and thus free from related deleterious effect, such as based on monitoring the dynamics of trapped atoms [31,32] or ions [33,34], or of microscopic objects [35,36]. It is to the best of our knowledge state-of-the-art for surface force measurements.

This high sensitivity associated with the control of the distance to the mirror allows us to perform sensitive force measurements at its vicinity. By performing interleaved differential measurements close to the mirror and further away at a distance of 300 μm, we suppress the gravity force and any long-range bias on the force, such a parasitic vertical dipole force from the IR transverse confinement beam. This dipole force has been evaluated by varying the IR power as an offset of the order of 3×10^{-29} N with no resolved dependence on the distance to the mirror. These differential force measurements, displayed as blue circles in Fig. 4, exhibit a clearly attractive behavior. As a reference, the effect expected from the Casimir-Polder force is also displayed as a green curve. It was calculated using the energy shifts of the Wannier Stark states due to the Casimir-Polder interaction, as computed in [37] for our exact experimental configuration. From a simulation of the fringe

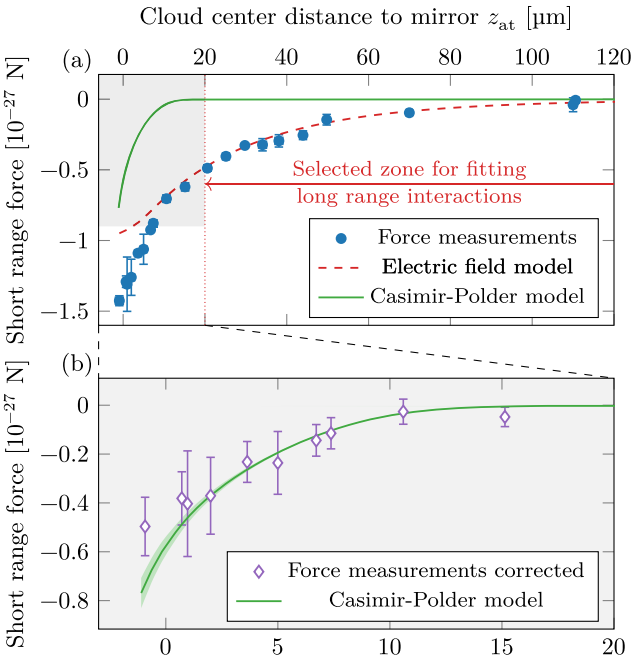

FIG. 4. Force measurements close to the mirror surface. (a) Blue circles: raw force measurements. Dashed red: fit to these above 20 μm by a model of the interaction with a Gaussian distribution of electric dipoles. Green line: expected Casimir-Polder force. (b) Purple diamonds: corrected force measurements. The error bars denote the 1σ statistical errors.

patterns averaged over the finite size of the cloud, we extract the frequency shift of the central fringe, and the corresponding expected force.

The observed force, which has a longer range and greater magnitude, cannot be explained by the Casimir-Polder effect alone. Another interaction is at play, likely due to electrostatic interactions between our atomic sample and electric dipoles by atoms adsorbed on the dielectric surface, as already put into evidence in [38].

Rb atoms adsorbed on neutral surfaces create dipole electric moments whose value has been evaluated to $\mu = 3.2$ D in [39] for a silica substrate. An atom brought near the surface thus experiences an attractive potential $U_{\text{elec}} = (\alpha_0/2)|\vec{E}|^2$, where α_0 is the static polarizability of the atom ground state and $\vec{E}$ is the electrostatic field produced by these moments, and thus experiences the force $\vec{F}_{\text{elec}} = -(\alpha_0/2)\vec{\nabla}|\vec{E}|^2$, to the vertical component of which our sensor is sensitive.

We observed a reduction by half of the force measured above 20 μm, where the Casimir-Polder effect is weak, by simply turning off the experiment for a month. It then returned to a new steady state after a week of operation. We interpret this as a first evidence of the stray electric fields from adsorbed atoms, which slowly desorb or diffuse, as already demonstrated in [39].

Furthermore, applying uniform vertical external electric fields E^z_{ext} using electrodes surrounding the mirror as shown Fig. 2 amplifies the force F^z_{elec} by $-\alpha_0 E^z_{\text{ext}} \mathrm{d}_z E^z$ and allows for measuring vertical gradients of the parasitic electric field $\mathrm{d}_z E^z$. The vertical electric gradient at a distance of 20 μm was found to be $2.0(1) \times 10^7$ V/m^2, of order of the gradient expected from a model described below [$3.3(4) \times 10^7$ V/m^2].

To model these parasitic electric fields, we consider a Gaussian distribution of N dipole moments over an rms radius σ_r: $n(r) = N/(2\pi\sigma_r^2)\exp[-r^2/(2\sigma_r^2)]$. The resulting electrostatic force along the vertical direction depends only on the two parameters N and σ_r [28] which we estimate by fitting our force measurements in the range $z > 20$ μm where the Casimir-Polder force is negligible, see Fig. 4. We get σ_r around 90 μm, a radius twice as large as the radial width of the atomic cloud at the end of the transport, and a number of adsorbed atoms N around 2.0×10^{10}, compatible with a continuous launch of atoms over several weeks and a significant fraction of the atoms not stopped at the end of the transport [26].

Finally, by using this estimated bias electrostatic force to correct our force measurements over the full range, we obtain good agreement between corrected measurements, depicted with diamond points in Fig. 4(b), and the expected Casimir-Polder force in the range $z < 20$ μm. Note though that this subtraction increases significantly the error bars for the corrected force measurements, which now take into account the uncertainties in the fit parameters. We also display as a green area the uncertainty in the expected force, related to uncertainties in the key parameters of the calculation (such as the size of the atomic sample and the Raman coupling).

Remarkably, we obtain here the first direct measurement of the Casimir-Polder force (rather than its gradient) in this micrometric range of distances, and, in particular, across the transition, situated at about 3–4 μm, between the Casimir-Polder regime and the Lifshitz regime where thermal contributions impact the amplitude of the force and its scaling with distance.

In conclusion, we performed state-of-the art short range force measurements, using an atom interferometer based on a fully trapped geometry. We made one of the very few demonstrations of a true competitive advantage in terms of performance of trapped schemes with respect to free falling ones [19,40], and the first measurement beyond the capability of free fall interferometers of an actual force in a fully trapped atom interferometer. In the regime of distance explored, the force is dominated by electrostatic forces from adsorbed atoms, but we achieved an evidence of the Casimir-Polder force in the micrometer range. A thorough characterization of stray electric fields would allow for a better comparison between expected and measured Casimir-Polder forces, opening the way for tests of gravity at short range. The removal, or at least the reduction of the number of adsorbed atoms, thanks to the heating of the surface [39] would be an asset for such

studies. The spatial resolution could be improved, by starting with smaller clouds or implementing a spatial selection by lifting the degeneracy between Wannier-Stark transitions, for instance, by using magnetic field gradients [41], or by shaping the trapping potential as a superlattice [42]. The resulting loss in detected atom number could be mitigated by improving the efficiency of the atom transport and recapture. This would allow for more sensitive and better resolved measurements of atom-surface interactions.

Acknowledgments—We thank Xiaobing Deng for early contributions, and A. Maury, M. Donaire, M.-P. Gorza, A. Lambrecht, and R. Guérout for providing us with the calculations of the energy levels in our system. This research has been carried out in the frame of the QuantERA project TAIOL, funded by the European Union's Horizon 2020 Research and Innovation Programme and the Agence Nationale de la Recherche (ANR-18-QUAN-0015-01).

Y. B. and L. A. contributed equally to this work.

[1] P. Wolf, P. Lemonde, A. Lambrecht, S. Bize, A. Landragin, and A. Clairon, Phys. Rev. A **75**, 063608 (2007).
[2] I. Antoniadis, S. Baessler, M. Büchner, V. Fedorov, S. Hoedl, A. Lambrecht, V. Nesvizhevsky, G. Pignol, K. Protasov, S. Reynaud, and Y. Sobolev, C. R. Phys. **12**, 755 (2011).
[3] H. B. G. Casimir and D. Polder, Phys. Rev. **73**, 360 (1948).
[4] D. Raskin and P. Kusch, Phys. Rev. **179**, 712 (1969).
[5] A. Laliotis, B.-S. Lu, M. Ducloy, and D. Wilkowski, AVS Quantum Sci. **3**, 043501 (2021).
[6] C. I. Sukenik, M. G. Boshier, D. Cho, V. Sandoghdar, and E. A. Hinds, Phys. Rev. Lett. **70**, 560 (1993).
[7] C. Garcion, N. Fabre, H. Bricha, F. Perales, S. Scheel, M. Ducloy, and G. Dutier, Phys. Rev. Lett. **127**, 170402 (2021).
[8] D. Bloch and M. Ducloy, *in Advances In Atomic, Molecular, and Optical Physics* (Elsevier, New York, 2005), Vol. 50, pp. 91–154.
[9] T. Peyrot, N. Šibalić, Y. R. P. Sortais, A. Browaeys, A. Sargsyan, D. Sarkisyan, I. G. Hughes, and C. S. Adams, Phys. Rev. A **100**, 022503 (2019).
[10] A. Landragin, J.-Y. Courtois, G. Labeyrie, N. Vansteenkiste, C. I. Westbrook, and A. Aspect, Phys. Rev. Lett. **77**, 1464 (1996).
[11] H. Bender, P. W. Courteille, C. Marzok, C. Zimmermann, and S. Slama, Phys. Rev. Lett. **104**, 083201 (2010).
[12] D. M. Harber, J. M. Obrecht, J. M. McGuirk, and E. A. Cornell, Phys. Rev. A **72**, 033610 (2005).
[13] S. Pelisson, R. Messina, M.-C. Angonin, and P. Wolf, Phys. Rev. A **88**, 013411 (2013).
[14] S. Dimopoulos and A. A. Geraci, Phys. Rev. D **68**, 124021 (2003).
[15] I. Carusotto, L. Pitaevskii, S. Stringari, G. Modugno, and M. Inguscio, Phys. Rev. Lett. **95**, 093202 (2005).
[16] F. Sorrentino, A. Alberti, G. Ferrari, V. V. Ivanov, N. Poli, M. Schioppo, and G. M. Tino, Phys. Rev. A **79**, 013409 (2009).
[17] Q. Beaufils, G. Tackmann, X. Wang, B. Pelle, S. Pelisson, P. Wolf, and F. P. dos Santos, Phys. Rev. Lett. **106**, 213002 (2011).
[18] X. Alauze, A. Bonnin, C. Solaro, and F. P. D. Santos, New J. Phys. **20**, 083014 (2018).
[19] M. G. Tarallo, T. Mazzoni, N. Poli, D. V. Sutyrin, X. Zhang, and G. M. Tino, Phys. Rev. Lett. **113**, 023005 (2014).
[20] T. Zhang, L.-L. Chen, Y.-B. Shu, W.-J. Xu, Y. Cheng, Q. Luo, Z.-K. Hu, and M.-K. Zhou, Phys. Rev. Appl. **20**, 014067 (2023).
[21] C. D. Panda, M. Tao, M. Ceja, A. Reynoso, and H. Müller, Appl. Phys. Lett. **123**, 064001 (2023).
[22] G. M. Tino, Proc. Int. Sch. Phys. Fermi **188**, 457 (2014).
[23] M. Harlander, M. Brownnutt, W. Hänsel, and R. Blatt, New J. Phys. **12**, 093035 (2010).
[24] C. P. Blakemore, A. D. Rider, S. Roy, Q. Wang, A. Kawasaki, and G. Gratta, Phys. Rev. A **99**, 023816 (2019).
[25] A. O. Sushkov, W. J. Kim, D. A. R. Dalvit, and S. K. Lamoreaux, Phys. Rev. Lett. **107**, 171101 (2011).
[26] L. Absil, Y. Balland, and F. P. D. Santos, New J. Phys. **25**, 073010 (2023).
[27] B. Pelle, A. Hilico, G. Tackmann, Q. Beaufils, and F. Pereira dos Santos, Phys. Rev. A **87**, 023601 (2013).
[28] See Supplemental Material at http://link.aps.org/supplemental/10.1103/PhysRevLett.133.113403 for additional details.
[29] G. Tackmann, B. Pelle, A. Hilico, Q. Beaufils, and F. Pereirados Santos, Phys. Rev. A **84**, 063422 (2011).
[30] J. Le Gouët, T. Mehlstäubler, J. Kim, S. Merlet, A. Clairon, A. Landragin, and F. Pereira Dos Santos, Appl. Phys. B **92**, 133 (2008).
[31] S. Schreppler, N. Spethmann, N. Brahms, T. Botter, M. Barrios, and D. M. Stamper-Kurn, Science **344**, 1486 (2014).
[32] X. Guo, Z. Yu, F. Wei, S. Jin, X. Chen, X. Li, X. Zhang, and X. Zhou, Sci. Bull. **67**, 2291 (2022).
[33] M. J. Biercuk, H. Uys, J. W. Britton, A. P. VanDe-vender, and J. J. Bollinger, Nat. Nanotechnol. **5**, 646 (2010).
[34] K. A. Gilmore, M. Affolter, R. J. Lewis-Swan, D. Barberena, E. Jordan, A. M. Rey, and J. J. Bollinger, Science **373**, 673 (2021).
[35] J. Moser, J. Güttinger, A. Eichler, M. J. Esplandiu, D. E. Liu, M. I. Dykman, and A. Bachtold, Nat. Nanotechnol. **8**, 493 (2013).
[36] D. Hempston, J. Vovrosh, M. Toroš, G. Winstone, M. Rashid, and H. Ulbricht, Appl. Phys. Lett. **111**, 133111 (2017).
[37] A. Maury, M. Donaire, M.-P. Gorza, A. Lambrecht, and R. Guérout, Phys. Rev. A **94**, 053602 (2016).
[38] J. M. McGuirk, D. M. Harber, J. M. Obrecht, and E. A. Cornell, Phys. Rev. A **69**, 062905 (2004).
[39] J. M. Obrecht, R. J. Wild, and E. A. Cornell, Phys. Rev. A **75**, 062903 (2007).

[40] C. D. Panda, M. J. Tao, M. Ceja, and H. Müller, Nature (London) **631**, 515 (2024).

[41] D. Schrader, I. Dotsenko, M. Khudaverdyan, Y. Miroshnychenko, A. Rauschenbeutel, and D. Meschede, Phys. Rev. Lett. **93**, 150501 (2004).

[42] F. Pereira Dos Santos, P. Wolf, A. Landragin, M.-C. Angonin, P. Lemonde, S. Bize, A. Clairon, A. Lambrecht, B. Lamine, and S. Reynaud, in *Frequency Standards and Metrology* (World Scientific, Singapore, 2009), pp. 44–52.